8-2020

Through-the-wall Radar Detection Using Machine Learning

Aihua W. Wood

Ryan Wood

Matthew Charnley

Results in Applied Mathematics 7 (2020) 100106

Contents lists available at ScienceDirect

Results in Applied Mathematics

journal homepage: www.elsevier.com/locate/results-in-applied-mathematics

Through-the-wall radar detection using machine learning

Aihua Wood [a,*], Ryan Wood [b], Matthew Charnley [c]

[a] Department of Mathematics and Statistics, Air Force Institute of Technology, 2950 Hobson Way, Wright-Patterson AFB, OH 45433, United States

[b] Department of Statistics, Harvard University, Cambridge, MA 02138, United States

[c] Department of Mathematics, Rutgers University, 110 Frelinghuysen Road Piscataway, NJ 08854, United States

ARTICLE INFO

Article history:
Received 23 January 2020
Received in revised form 1 April 2020
Accepted 10 April 2020
Available online 27 April 2020

ABSTRACT

This paper explores the through-the-wall inverse scattering problem via machine learning. The reconstruction method seeks to discover the shape, location, and type of hidden objects behind walls, as well as identifying certain material properties of the targets. We simulate RF sources and receivers placed outside the room to generate observation data with objects randomly placed inside the room. We experiment with two types of neural networks and use an 80-20 train-test split for reconstruction and classification.

1. Introduction

Detection and description of objects behind walls is an important area of research due to its obvious physical and engineering applications. One particular approach is the use of radar frequency imaging to retrieve the properties of an unknown object from its back-scattered fields. Previous work has used Doppler-type radar to detect and analyze humans where there is no direct line of sight, whether it be studying human motion with standard Doppler radar [1], noiseforms [2], or micro-Doppler radar, which looks for smaller scale movements such as arm movement [3] and heartbeats [4]. In [5], a Support Vector Machine approach was used to discriminate between child and adult in a through-the-wall setting. More recent work in [6,7] used a similar approach to get more detailed results, using the back-scattered data to estimate the pose of a human figure behind a wall, or detect that the figure is walking.

In [8], locations of hidden objects behind walls were estimated by observing the time difference between signals from an empty room and that when an object is present. Based on the physics of electromagnetic wave propagation, ellipses with foci at the source and receiver pairs were constructed to provide the contour of the objects. In [9], a form of linear sampling method was used for the reconstruction. Specifically, a reciprocity gap functional to the electromagnetic field solution and the fundamental solution of the Helmholtz equation was used to derive an integral equation, the properties of whose solution gave indication of the location of the objects. This work explores a machine learning (ML) approach for three objectives:

(1) predicting the location of an object,
(2) classifying the shape of an object into one of a number of known possible shapes, and
(3) estimating a particular material property of an object.

* Corresponding author.
E-mail addresses: aihua.wood@afit.edu (A. Wood), rwood@college.harvard.edu (R. Wood), charnley@math.rutgers.edu (M. Charnley).

https://doi.org/10.1016/j.rinam.2020.100106

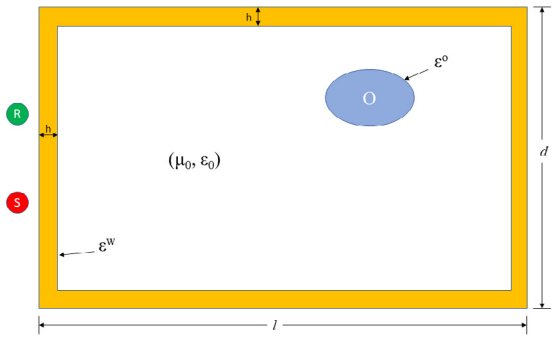

Fig. 1. Model setup.

The reconstructions use similar RF data as in [8,9], which was generated by numerically modeling the Maxwell's equations. We note that [8,9] used traditional inverse methods to reconstruct the shape and location of the unknown objects by identifying points within the contours of the objects. In the ML approach here, we reconstruct the locations of the unknown objects by identifying their geometric centers. In addition, the ML algorithms are capable of classifying different objects and reconstructing certain material properties of the unknown objects. We present reconstruction results from two popular ML algorithms and compare the location identification results to those reported in [8,9].

We note that using ML to detect unknown objects, or detect structural defects, is not new, see for example [10]. However, to the best of our knowledge, this is the first attempt reported in the open literature that ML is used in the behind-the-wall setting employing the numerically simulated data from solving Maxwell's equations. Our preliminary results show promise that ML can significantly improve the state-of-the-art of the inverse scattering methods, and produce estimators for characteristics that were previously nonexistent.

The rest of the paper is organized as follows. In the next section, we summarize the forward problem of data generation with a discussion of the model setup, the mathematical formulation, and the numerical schemes. Section 3 provides preliminaries for our machine learning approach, including preparing the data, setting the parameters, and identifying appropriate neural networks. Section 4 shows the reconstruction results with comparisons to those of the previous methods. Object classification is presented in Section 5, while target material property reconstruction in Section 6. We conclude our paper with comments and suggestions for follow on research.

2. Data generation

To model the actual physical problem, we will record and use data that could be gathered from a set of antenna transmitters and receivers. Thus, for any given simulation, we will assume that the electromagnetic waves are generated from a source antenna (S) positioned outside of the room and the data is recorded from a (finite) set of receivers (R), also positioned outside the room as shown in Fig. 1.

We consider a two-dimensional radar imaging problem, assuming that all materials are invariant in the z-direction. The room is rectangular of size l by d. The walls are of a uniform thickness h, with relative electric permittivity ϵ^w. The object that is to be detected is a convex domain $O \subset [0, l] \times [0, d]$ that has relative electric permittivity ϵ^o and is away from the boundaries of the room. We assume the medium throughout is nonmagnetic, thus $\mu_r = 1$. The source will be monochromatic with frequency ω, emitting two full cycles of the wave before turning off. We observe that $k = \omega\sqrt{\mu\epsilon}$ and $\lambda = c_0/\sqrt{\epsilon_r}\omega$, where k is the wavenumber, ω frequency, λ wavelength, and c_0 free space speed of light.

For our experiments shown in this paper, we choose $\epsilon^w = 80$, $\omega = 600$ MHz. The Perfectly Matched Layer (PML) used in the numerical simulation will be placed along the exterior of the room, .5m from the walls.

Our simulated data will be obtained in two ways. The first is via simulating the solutions to the time domain Maxwell's equations, while the second solutions of the corresponding Helmholtz equation via Lippmann–Schwinger integral equation. Two techniques were used because although the first technique is computationally less intensive with constant material conductivity than the second technique, the first technique becomes computationally prohibitive when the material conductivity parameter is varied. For this reason, we use the first technique to generate a large dataset with a constant material parameter for building models to estimate the shape and location of an object, but we use the second technique to generate a dataset for building models to estimate the conductivity parameter of an object. Below, we briefly describe the two numerical schemes. The reader is referred to [8,9,11] for details.

2.1. Maxwell's equation

Consider Maxwell's equations in the absence of free charges:

$$\begin{cases} \frac{\partial \vec{E}}{\partial t} = \frac{1}{\epsilon}\nabla \times \vec{H} \\ \frac{\partial \vec{H}}{\partial t} = -\frac{1}{\mu}\nabla \times \vec{E} \\ \nabla \cdot \vec{E} = 0 \\ \nabla \cdot \vec{H} = 0 \end{cases}$$

Since the problem is assumed invariant in the z direction, solutions to the scattering problem can be expressed as linear combinations of the two fundamental polarizations: transverse magnetic (TM) and transverse electric. We consider the TM case, where only the fields E_z, H_x, and H_y are non-zero. Therefore, we need only consider the following 3 partial differential equations

$$\begin{cases} \frac{\partial E_z}{\partial t} = \frac{1}{\epsilon}\left(\frac{\partial H_y}{\partial x} - \frac{\partial H_x}{\partial y}\right) \\ \frac{\partial H_x}{\partial t} = -\frac{1}{\mu}\frac{\partial E_z}{\partial y} \\ \frac{\partial H_y}{\partial t} = \frac{1}{\mu}\frac{\partial E_z}{\partial x} \end{cases} \tag{1}$$

We use a finite difference scheme to approximate the Eqs. (1). For best accuracy, we use a centered difference approximation for every derivative in (1). We observe that for general electromagnetism problems, it would be safe to assume that the component functions of $\vec{H}$ and $\vec{E}$ are C^3, thus securing the second order accuracy of the finite difference time domain (FDTD) scheme. For material interfaces, such as objects/space and space/wall, we use an averaging method to make these parameters continuous. Specifically, as the point (x, y) moves in or out of the object, the permittivity changes accordingly. We construct a square S around the point (x, y) with side length equal to our grid spacing in the Yee Scheme [12,13], with (x, y) at the center. We then define our smoothed permittivity as the average value of the permittivity on S, namely

$$\tilde{\epsilon}(x, y) = \frac{1}{|S|}\int_S \epsilon(r, t)\, dr\, dt.$$

Another issue of concern in data generation has to do with domain truncation. Since the scattering problem is infinite in nature, we use the PML [14,15] to truncate the computational domain to avoid nonphysical reflections at the boundary. The idea of PML is to add a layer of lossy material near the edge of the computational domain so that any waves heading towards the boundary decay away before they get there. Since the waves have decayed, we can then put a hard boundary at the edge of the computational domain ($E_z = 0$), causing a negligible reflection. It is also necessary to make the boundary of this region with the interior reflectionless so as to not significantly change the value of the wave in the internal region.

We observe that the portion of a wave incident on an interface that is reflected at the boundary is determined by the impedance of the material

$$\eta = \sqrt{\frac{\mu^*}{\epsilon^*}}.$$

If the impedance of the material on both sides of an interface are equal, there will be no reflection at that interface, and the entire wave will be transmitted. We know the impedance on the plain material side is $\sqrt{\frac{\mu}{\epsilon}}$. In order to make the media reflectionless, we define new permeability and permittivity such that $\epsilon^* = 1$ outside the PML region, while inside the region the waves decay rapidly.

2.2. Lippmann–Schwinger equation

In the case of time-harmonic waves in the TM mode, the electric field can be expressed as

$$\vec{E}(x, t) = \vec{u}(x)e^{i\omega t} = (0, 0, u)e^{i\omega t},$$

reducing Maxwell's equations to

$$\begin{cases} \Delta u + k^2 u = 0 & x \in \mathbb{R}^2 \\ u = u^i + u^s & \\ \lim\limits_{r\to\infty} \sqrt{r}\left(\frac{\partial u^s}{\partial r} - iku\right) = 0 & \end{cases} \tag{2}$$

where $k^2 = \omega^2\epsilon_0\mu_0 n$, n is the index of refraction, u^i the incident field, u^s the scattered field.

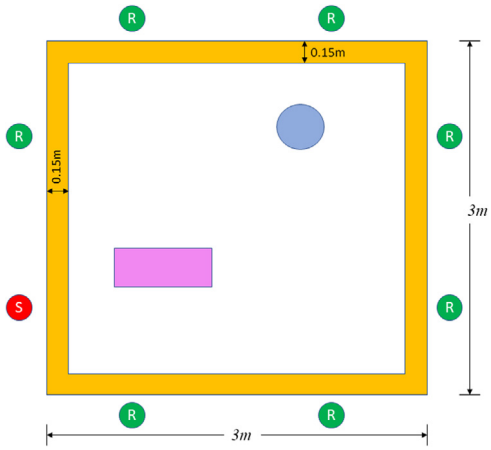

Fig. 2. Machine learning setup.

It can be shown, [16], that solution to (2) satisfies the Lippmann–Schwinger equation

$$u(x) = u^i - k^2 \int_{\mathbb{R}^2} \Phi_x(y) m(y) u(y)\, dy \tag{3}$$

where $m := 1 - n$ has compact support and $\Phi_x(y) = \frac{i}{4} H_0^{(1)}(k|x-y|)$ is the fundamental solution of the free-space Helmholtz equation

$$\Delta u + k^2 u = 0.$$

The solution of (3) anywhere in $\mathbb{R}^2$ can be found once we know the solution on the object (as $m = \frac{i\sigma}{\omega} = 0$ away from the object). With proper truncation of the integral to account for the singularity of $\Phi_x(x)$ and restrict to the grid points, we can write Eq. (3) as a matrix equation

$$(I + K)\vec{u} = \vec{u}^i$$

and generate our needed data by solving this equation.

This data will be used to reconstruct the material parameter, k, the unknown object's wave number.

3. Machine learning setup

For target reconstruction and classification, our data is the time series real component of the electric field profile recorded at each of the receivers. One source and a varied number of receivers are placed at even intervals outside a square (3 m by 3 m) room. Objects of different types and sizes are uniformly randomly placed inside the room. For computational tractability in the data simulation, all objects are placed so that they are not touching the walls. See Fig. 2. Data is generated by numerical simulations as described in Section 2. An 80–20 training–testing data-split is adopted.

In what follows we will use two types of algorithms for the reconstruction of unknown targets: 1. a pattern recognition algorithm, K-Nearest Neighbors (K-NN), and 2. a Convolutional Neural Network (CNN) using *Keras-TensorFlow*. K-NN was chosen because it is particularly flexible and can be easily applied to a wide range of problems, and thus provides a robust benchmark for evaluating other machine learning methods. The CNN is designed to work well with problems where the features are spatially related to each other. Because the receivers are evenly spaced around the perimeter of the room, their measurements are spatially dependent on measurements of nearby receivers. The collected data also consist of a second dimension in time. Measurements taken by the same receiver at two similar times are also correlated with each other. Unraveling this 2-dimensional time series data into a 2-D array yields data in which each measurement is correlated with the measurements near it in either dimension. This form of data fits the construction of a convolutional neural network nicely.

3.1. The K-Nearest Neighbors algorithm

The K-NN is one of the simplest machine learning algorithms that can be used for both regression and classification tasks. It is nonparametric, making it extremely flexible compared to other classical regression and classification techniques, such as linear regression and logistic regression. Easy to interpret and quick to implement, K-NN does not require data preparation, and often yields performance in regression and classification tasks that are difficult to beat, even compared to

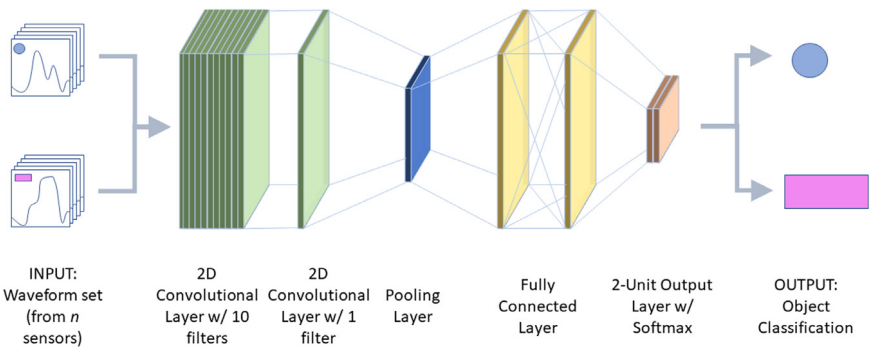

Fig. 3. Convolutional neural network structure.

some of the state-of-the-art deep learning techniques. Two of K-NN's main shortcomings are: 1. Large amounts of densely distributed training data are required for good performance; 2. The entire training set is required for each prediction. See [17]. However, since the experiment uses simulated data, provided adequate computational power, arbitrarily large amounts of data can be acquired, alleviating the first issue. The second issue is solved by simply carrying out the experiment on a machine with sufficient resources.

3.2. Convolutional neural network structure

We observe that CNN is best suited for analyzing visual imagery. Our "image" for each observation is the time-series data for all receivers, resulting in a predictor matrix of $m \times n$, where m is the number of receivers and n, the number of time steps. We monitor the accuracy rates of the training–testing data as the network runs through each *epoch*, of the entire dataset, and terminate when either a desired accuracy is reached or the improvement stalls.

For activation function, we choose ReLU: $x \to \max\{0, x\}$, for its advantages of sparse neuron activation and efficiency. For the loss layer, we choose Softmax: $y_i \to \frac{e^{y_i}}{\Sigma_i e^{y_i}}$, as it is suitable for predicting a single class of a fixed number (2 in our case) of mutually exclusive classes.

Fig. 3 shows the layer structure of our CNN in the *Keras-TensorFlow* framework. The convolutional and fully connected layers are each equipped with a ReLU activation function.

4. Object reconstruction

We use K-NN for object reconstruction. The main reason for this choice is its ease of adaptation and potential for good performance in many applications, giving it merit as a benchmark for evaluating the CNN described later. Since our data is generated by simulation, the density of the data for training can be very large, given enough computing power. Thus the lack of efficiency (in both time and memory), a main disadvantage of K-NN, is not of major concern.

For our experiment, each observation was obtained by setting the type of object to be placed in the room, and randomly assigning a location within the room. Three types of objects were considered: small circle of radius 0.1 m, small rectangle of size 0.1 m $\times$ 0.2 m, and large rectangle of size 0.3 m $\times$ 0.6 m. Data for each object were collected. Symmetries in the data were also used; the locations of the objects were initialized to be in the top half of the room, then the simulations run, and data for an object in the same location on the bottom half of the room were inferred by switching the readings of the receivers appropriately. In all, over 10,000 observations were generated, taking up about 16 GB of storage.

Example 1. For this experiment, we placed 6 receivers behind the left wall, taking data at 100 time steps. This yielded 1164 observations with $6 \times 100 = 600$ predictors. Using $k = 1$ nearest neighbor, the average L2-norm distance between predicted and actual location of a circular object with radius 0.1 m was only 0.1049 m, and the variance was 0.0501 m. It took 0.044528 s for each run. See Fig. 4.

Example 2. In this experiment, both the sources and receivers are placed on one side of the room only. This is perhaps more applicable given that it may only be possible to access one external wall of the room. We compare this partial reconstruction of ML, K-NN in this case, to that of the linear sampling method (LSM). The LSM is a well known mathematical method for solving inverse scattering problems, see [18]. Fig. 5 shows predictions by LSM of a circle object with data from one side of the room. In this case, we see that for every point the algorithm identifies as the object, there is a shadow cast behind it. This is expected, since without data from the other sides of the room there is no way to determine where the object ends in that direction.

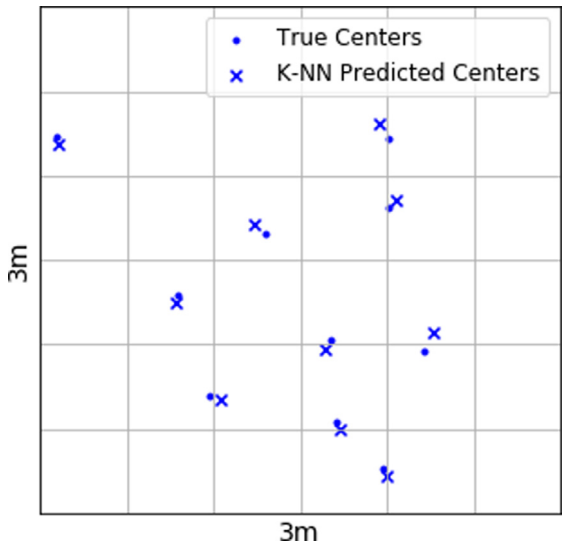

Fig. 4. Illustration of the centers (crosses) of randomly placed circular objects with radius 0.1 m, and predictions of the centers by K-NN (dots).

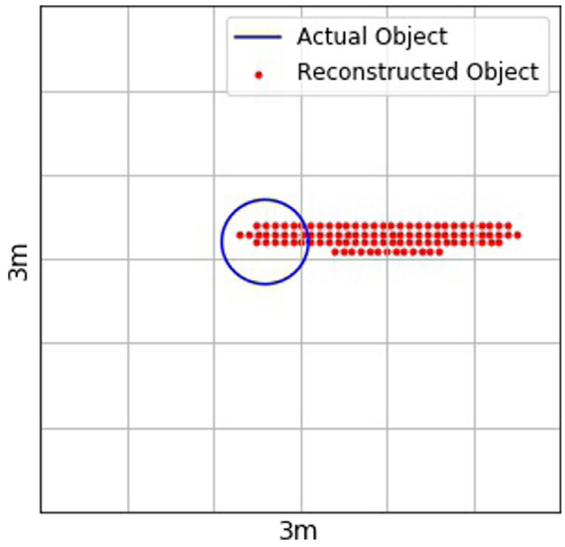

Fig. 5. Illustration of the true shape and location of a circular object, and its reconstruction by LSM (red dots).

For circle objects of radius 0.1 m, K-NN returned prediction error of the same order as the radius when 24 receivers were used, and only double that with a total of just 3 receivers placed on one side of the external wall. See Fig. 6.

We observe that placing 24 receivers evenly along all sides of the room produced better results than placing them all on one side. This is not surprising since partial "visibility" from all sides often is better than a "full" vision from only one side.

5. Object classification

For object classification, we experimented with both the simple pattern recognition algorithm, K-NN, and the deep learning network, CNN via Keras-TensorFlow. The CNN network was trained with our simulated radar data.

We observe that neither K-NN nor the CNN could distinguish different shapes (rectangles versus circles) when the difference in relative sizes (i.e. area, side length, radii) were not sufficiently large. However, when the size of one object was increased so that the side length of the rectangular object was at least double or at most half of the radius of the circular object, both algorithms saw significant improvements in accuracy.

Number of receivers	24	12	6	3
Average error	0.1523	0.1386	0.2440	0.2764
Variance of error	0.1202	0.1565	0.2518	0.2921

Fig. 6. Sources & receivers on one side of room by K-NN.

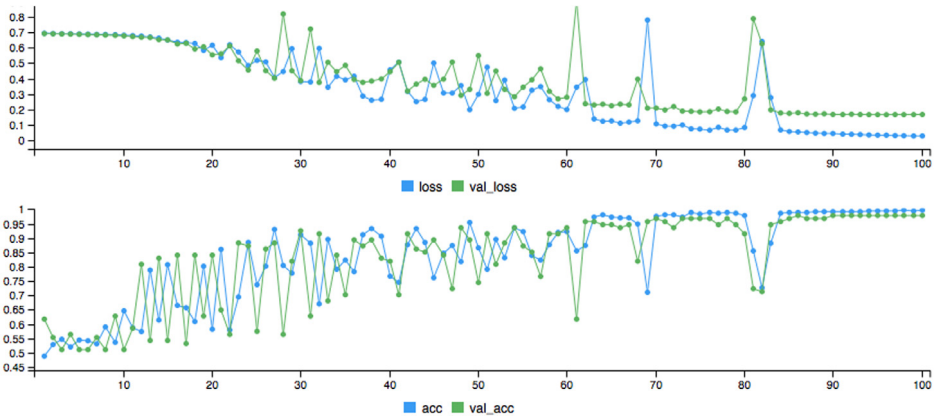

Fig. 7. Accuracy and loss vs. epoch.

The data for each observation were prepared in the following way: the time-series data for each of 28 evenly spaced receivers behind the left wall of the room were put into each of 28 rows of a matrix, and the time steps were sampled at a rate of 1/5, giving a 28×40 predictor matrix.

With this data, K-NN returned a 97% accuracy rate. Meanwhile, our CNN reached $>$ 99% accuracy rate on the 20% testing data after 100 epochs of training on the other 80% of the data. The training and validation accuracies and losses after each of 100 total epochs, are plotted in Fig. 7.

6. Reconstruction of target material property

Our next set of experiments attempt to reconstruct the target material properties. In particular, using simulated data obtained by numerically solving the Lippmann–Schwinger equation (3), we employed our neural networks to reconstruct the wave number k. Our results show that K-NN does a good job of approximation in the simple case of circles of fixed location and fixed radius, but fails when the data structure becomes more complex. Specifically, when we allow circles of various radii to be placed at random locations, K-NN produced random results. However, our deep learning network, the CNN via Keras-TensorFlow produced impressive results after adequate training. Fig. 8 is a plot showing the training/testing process of predicting the target material parameter k in the range of $20 < k < 100$. It shows that after 200 epochs, the average error reaches below 6. We note that for objects with k parameters uniformly distributed between 20 and 100, a baseline model that predicts a constant value has an optimal expected absolute error of 20, so the machine learning model's average absolute error of 6 units reflects a substantial improvement.

7. Conclusion

Through-the-wall object detection is an important area of research that has a wide range of physical and engineering applications. By utilizing both a simple pattern recognition algorithm, K-NN, and a deep convolutional neural network, we have reconstructed unknown targets behind walls using the same FDTD and LSM data used by our previous traditional inverse methods more accurately and with less time. In addition, our ML models are capable of classifying different types of objects and determining material properties of the targets that the other reconstruction methods do not attempt. Moving forward, we would be interested in exploring more complex settings including multiple objects, multiple reflections, and moving targets, to name a few.

Declaration of competing interest

The authors declare that they have no known competing financial interests or personal relationships that could have appeared to influence the work reported in this paper.

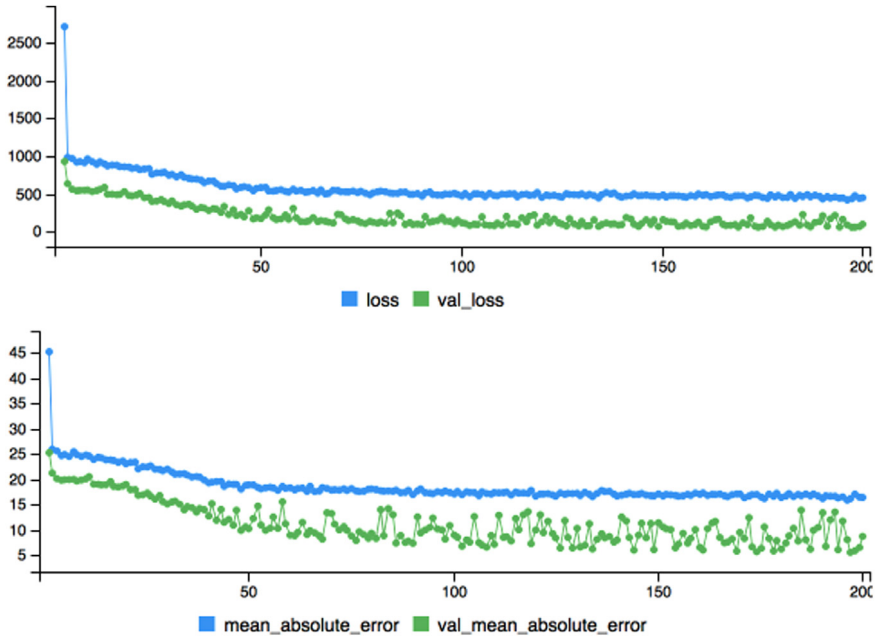

Fig. 8. Prediction of target material property: k.

Acknowledgments

Much of the work was done while the first author was sabbatical at Oxford University with support from AFOSR, United States. We thank Phillipp Petersen for many insightful discussions, and Paul Rudolph for valuable graphical support.

The authors thank the anonymous reviewers for the very helpful comments and suggestions.

References

[1] Ram SS, Li Y, Lin A, Ling H. Doppler-based detection and tracking of humans in indoor environments. J Franklin Inst B 2008;356(6):679–99, Advances in Indoor Radar Imaging.
[2] Narayanan RM. Through-wall radar imaging using UWB noise waveforms. J Franklin Inst B 2008;345(6). 689-678. Advances in Indoor Radar Imaging.
[3] Narayanan RM, Shastry MC, Chen PH, Levi M. Through-the-wall detection of stationary human targets using doppler radar. Prog Electromatnetics Res B 2010;20:147–66.
[4] Bugaev AS, Chapursky VV, Ivashov SI, Razevig VV, Sheyko AP, Vasilyev IA. Through wall sensing of human breathing and heart beating by monochromatic radar. In: Ground penetrating radar, 2004. Proceedings of the tenth international conference on, Vol. 1. 2004, p. 291–4.
[5] Keith SR. Discrimination between child and adult forms using radar frequency signature analysis. AFIT-ENP-13-M-20, Air Force Institute of Technology; 2013.
[6] Adib M, Hsu C-Y, Mau H, Katsbi D, Durand F. Capturing the human figure through a wall newblock. ACM Trans Graph 2015;34.
[7] Zhao M, Li T, Alshekh MA, Tian Y, Zhao H, Torralba A, Katabi D. Computer vision and pattern recognition. 2018.
[8] Charnley M, Wood A. Through-the-wall radar detection analysis via numerical modeling of maxwell's equations. J Comput Phys 2016;313:532–48.
[9] Charnley M, Wood A. A linear sampling method for through-the-wall radar detection. J Comput Phys 2017;347:147–59.
[10] Joseph, Alguri K Supreet, Deemer Chris, Harley B. Structural damage detection using deep learning of ultrasonic guided waves. AIP Conf Proc 2018. http://dx.doi.org/10.1063/1.5031651.
[11] Charnley M, Wood A. Object Identification in Radar Imaging via the Reciprocity Gap Method Radio Science, 55 (1) (2019) 1-10.
[12] Kane S Yee. Numerical solution of initial boundary value problems involving maxwell's equations in isotropic media. 1966.
[13] Dennis M. Sullivan electromagnetic simulation using the FDTD method. IEEE; 2000.
[14] Berenger J-P. A perfectly matched layer for the absorption of electromagnetic waves. J Comput Phys 1994;114:185–200.
[15] Lassas M, Somersalo E. On the existence and convergence of the solution of PML equations. Computing 1998;60:229–41.
[16] Colton D, Kress R. Inverse acoustic and electromagnetic scattering theory, Vol. 3. New York: Springer-Verlag; 2013.
[17] Altman NS. An introduction to kernel and nearest-neighbor nonparametric regression. Amer Statist 1992;46(3):175–85.
[18] Colton D, Haddar H. An application of the reciprocity gap functional to inverse scattering theory. Inverse Problems 2005;21:383–98.